Duty Cycles Mathematical Analysis and Empirical Thrust-Force Performance Curves of a Brushless Electric Motor

Andra TOFAN-NEGRU[1]*, Amado ȘTEFAN[2], Cristian VIDAN[1,3]

[1] Centre of Excellence in Self-Propelled Systems and Technologies for Defence and Security, Military Technical Academy "Ferdinand I", 39-49 George Coșbuc Avenue, District 5, 050141, Bucharest, Romania
andra.negru@mta.ro (**Corresponding author*)

[2] Department of Aviation Integrated Systems and Mechanics, Military Technical Academy "Ferdinand I", 39-49 George Coșbuc Avenue, District 5, 050141, Bucharest, Romania
amado.stefan@mta.ro

[3] Doctoral School of Aerospace Engineering, Politehnica University of Bucharest, 313 Splaiul Independenței, 060042, Bucharest, Romania
cristian.vidan@mta.ro

Abstract: In recent years, research into the design, development and use of drones has been of great interest. In this paper, methods and equipment for testing electric motors in the operating regimes are presented. These types of brushless electric motors are mainly used in the equipment of rotary wing UAVs (unmanned aerial vehicles). Determining their performance curves is essential for correlating operating regime data with the response of the structure to the thrust force developed by the motor-propeller assembly. The mathematical analysis of the duty cycles data correlation with the rotor rotation speed involves the use of curve fitting and smoothing functions. To determine the thrust force developed by the motor-propeller assembly, a Wheatstone half-bridge was carried out, using strain gauges.

Keywords: Quadcopter arm, Tachometer, RPM, Linear regression function, Polynomial regression function, Residual diagram, Residual histogram, Strain gauge, Thrust force, Performance curve.

1. Introduction

Major advances have been made in UAV technology, exponentially increasing their development and the number of applications in which they are used. These aerial vehicles have overcome certain human limitations, managing to meet certain application requirements at lower costs and providing access to dangerous and hostile environments where humans do not have access (Balestrieri et al., 2021). UAVs present considerable advantages for supporting society, but also present a number of disadvantages in terms of the safety and security of the population, aspects that need to be addressed and resolved (Ayamga, Akaba, & Apotele Nyaaba, 2021; He et al., 2019).

During their missions, UAVs must avoid any danger that could endanger human life, ensuring safety and security (Fox, 2020). Continuous efforts to produce standards and regulations, to contribute to scientific research and to patents (Qu & Wu, 2016) are made to solve safety and security issues regarding UAVs. However, the dangers and risks of this type of air vehicle are still not fully known and understood, therefore taking appropriate countermeasures is not yet possible (ISO, n.d. a; Austin, 2010). Researches about controlling non-cooperative UAVs with the goal of minimizing damage caused by the rogue UAVs were made, analysing the mechanisms to counter UAVs and proposing novel method to build a no-fly zone for non-cooperative drones (He et al., 2019). Investigations on the uncertainty in the choice of preventive maintenance intervals with respect to the soft failure threshold have been carried out (Petritoli, Leccese & Ciani, 2018). The increased use of drones is accompanied by higher failure rates compared to conventional, manned aircraft (Petritoli, Leccese & Ciani, 2018). The operation of UAVs mainly depends on the types of sensors used in the equipment and the measurements that are made (Balestrieri et al., 2021; Daponte et al., 2017). Thus, sensor testing methods are essential resources that must be used to ensure the safety and security of drones.

The present research was carried out to determine the polynomial curve (Otkun, Demir & Otkun, 2022) that best fits the experimental measurements recorded in the duty cycles of the brushless electric motor (Dwivedi, Singh & Kalaiselvi, 2022). This curve is required to be introduced into the Catman software of a data acquisition chain from HBM to determine the real performance curve of the motor-propeller assembly (Meyer & Barros, 2021). The traction force developed by the motor-propeller assembly, for each motor operating regime, was used to determine the influence of the air jet produced by the propeller rotation movement on the quadcopter arm (Tofan-Negru et al., 2023). The variation of air flow produced by the propeller is an exciting factor in

https://doi.org/10.24846/v32i4y202308

inducing forced vibrations on the arm (Fu et al., 2022; ISO, n.d. b). Other influencing factors in the production of vibrations are represented by the static imbalance and the dynamic imbalance of the motor-propeller assembly. At present, there are few studies on reducing the amplitudes of forced vibrations induced in the quadcopter arm structure. So, the innovative character of this work is highlighted by the realization of the empirical test stand that allowed the simultaneous recording and fusion of the fluid velocity data around the quadcopter arm acquired with the hot wire anemometer, of the vibration velocity data acquired with laser vibrometer and tensile forces using the tensometric half-bridge. These data were determined for further use in the design of adapters for the quadcopter arm that aim to reduce vibration amplitudes, respectively to improve the dynamic response of the structure of the drone.

This research is based on the polynomial regression model, which is used when the relationship between two variables is curvilinear. The polynomial regression model was applied using the characterization of the relationship between the rotational speed and the duty cycle of the brushless electric motor that equips the arm of a quadcopter. Model parameters were estimated using the least squares method. After fitting, the model was evaluated using some of the common indicators used to assess the accuracy of the regression model. The data were analysed using the Mathcad computer program that allows this type of calculations to be made.

Regression analysis involves identifying the relationship between a dependent variable and one or more independent variables. This type of analysis is one of the most important statistical tools used in almost all sciences to study the relationship between two or more variables that are causally related. A model of the relationship is first derived, and estimates of the parameter values are used to develop an estimated regression equation. Afterwards, various tests are used to determine the validity of the model. This last step of model validation is very important in the modelling process, because it helps to assess the reliability of the models before they are used in decision making.

Section 2 presents the equipment and test methods used in the present research. Section 3 describes the engine performance curves with and without a mounted propeller obtained from the experimental measurements, and presents the mathematical interpretations using linear and polynomial regressions, the residual diagrams, and the residual histograms for the collected data. Section 4 addresses the determination of the thrust force that the motor-propeller assembly develops in the operating modes of the brushless electric motor, experiments in which a series of tests were carried out using two strain gauges for making a Wheatstone half-bridge. Section 5 is the final one and presents the conclusions of the present research.

2. Materials and Methods

The experimental tests carried out in the present research consisted in the determination of motor rotational speeds without propellers and with mounted propellers, measured in [RPM] (rotations per minute) and the determination of the thrust force developed by the motor-propeller assembly for the engine acceleration stages. The experimental setup for testing the quadcopter arm is shown in Figure 1, where the following

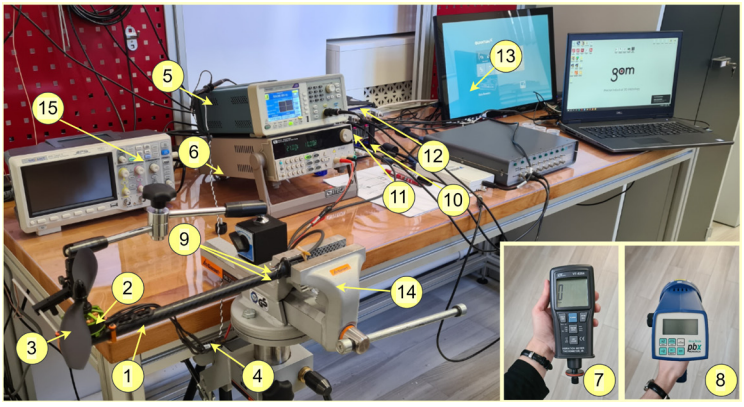

Figure 1. Experimental configuration for quadcopter arm testing

components of the equipment are illustrated: 1 – Quadcopter arm; 2 – Brushless electric motor; 3 – Propeller; 4 – Electronic Speed Controller; 5 – Signal generator; 6 – DC power supply; 7 – Contact tachometer; 8 – Stroboscope; 9 – Strain gauges; 10 – Data recorder; 11 – Strain gauge amplifier; 12 – Signal amplifier; 13 – Computer for CATMAN – HBM; 14 – Vise; 15 – Oscilloscope.

The experimental setup is divided into three equipment categories. Thus, the categorization marks the type of measurement for which the equipment was used.

The first category of equipment represents the starting stand which aims to drive the electric motor in the rotational movement and includes the following components:

- motor-propeller assembly, with TURNIGY Multistar 3508 640 v2 brushless electric motor and DJI 254x114mm Multistar propeller with adapter;

- HOBBYWING XRotorPro50A ESC (Electronic Speed Controller), used for controlling and regulating the electric motor speed;

- TEKTRONIX – AFG1062 signal generator (the square wave signal introduced for driving the motor had the following characteristics: frequency of 500Hz, duty cycle 50%, start phase 0°, amplitude 5Vpp, compensation 2.5V);

- ITECH IT6722A 400W with electrical supply 80V20A DC power supply (the 21V voltage and 10A intensity electric current were introduced to drive the electric motor).

The second category is represented by the equipment used for rotational speed determination of the engine operating regimes and includes the following components:

- LUTRON VT-8204 contact tachometer (the first equipment used for obtaining the duty cycles RPMs);

- Stroboscope Phaser-Strobe PBX (used for validating the RPMs measured with the tachometer).

The equipment used to obtain the thrust force generated by the motor-propeller assembly for the engine operating regimes represents the third category and contains the following components:

- HBM LY1 strain gauges – Standard strain gauge with leads = 1-LY1x-3/120 (used for making a Wheatstone half-bridge by which the relative elongations in the proximity of the quadcopter arm embedment area were determined);

- QuantumX CX22B-W data recorder from HBM (for collecting the measurement data);

- QuantumX MX1615B strain gauge amplifier from HBM (for amplifying the measurement data from the Wheatstone half-bridge).

3. Determination of Speeds in Engine Operating Modes

The revolutions data related to each engine operating mode are the first experimental data obtained. The first set of measurements was determined using the contact tachometer, and the second set, which validated the first collected data, was made with the stroboscope. The second set of measurements was carried to determine the actual RPM values for each engine throttle, knowing that the contact tachometer has the disadvantage of recording a lower value of the RPM than actual one, due to the frictional force that occurs between the contact surface of the equipment and the rotor. Also, the RPMs measurement could not be made using just the stroboscope, because capturing a stationary image of the propeller can represent both the actual RPM, but also 1/2, 1/3, 1/4, etc. from the real revolutions.

In the following, the engine performance curves with and without a mounted propeller obtained from the measurements, the mathematical interpretations using linear and polynomial regressions, the residual diagrams and the residual histograms for the collected data are presented.

3.1 Engine Speed Without Mounted Propeller

The performance curves of the engine without a mounted propeller, obtained from the tests carried out with the tachometer, are presented in this subsection. A linear regression was performed on the data recorded on the engine using the least squares method, thus obtaining the regression

line and the graph of the residuals (errors). The minimum value of the squares of the residuals was determined by the regression line.

Since the vector values of independent variables (exogenous) were considered the acceleration gear data, and since the dependent variable (endogenous) was considered the RPM, the coefficient of the independent variables vector was considered the value that returns the slope of the best-fitting line with the data from the percent throttle and RPM vectors and the free term was taken to be the value that returns the intercept of the line that best fits the data from the percent throttle and RPM vectors. Thus, the linear regression function will provide an equation of the form:

$$Y = r(X) = b_0 + b_1 \cdot X \tag{1}$$

which has the following components:

X = column vector of throttle percentage values;

Y = column vector of RPM values;

b_0 = the free term of the regression line (the value for X=0);

b_1 = regression coefficient (the amount by which Y changes when X changes by one unit).

Through the least squares method, it was obtained:

$$b_0 = \overline{Y} - b_1 \cdot \overline{X} = 1.145 \cdot 10^3 \tag{2}$$

$$b_1 = \frac{\sum\left(x_i - \overline{X}\right)\left(y_i - \overline{Y}\right)}{\left(x_i - \overline{X}\right)^2} = 118.395 \tag{3}$$

where $\overline{X} = \frac{x_1 + \ldots + x_n}{n}$ and $\overline{Y} = \frac{y_1 + \ldots + y_n}{n}$ represent the sample means, and n=45 represents the rows number of X and Y column vectors.

Accuracy depends on how closely the measured data points are spread around the regression line. The fit was assessed by performing a statistic: the standard error of the estimate, defined as the standard deviation of the estimate residuals:

$$s = \sqrt{\frac{1}{n-2}\sum\left[y_i - (b_0 + b_1 \cdot x_i)\right]^2} = 152.48 \tag{4}$$

An index independent of the number of values of X and Y vectors is the covariance calculated by the formula:

$$S_{xy} = \frac{1}{n-1}\sum_{i=1}^{n}\left(x_i - \overline{X}\right)\cdot\left(y_i - \overline{Y}\right) = 1.178 \cdot 10^5 \tag{5}$$

Pearson's correlation coefficient R is determined to measure the relationship between the values of X and Y and is expressed by:

$$R = \frac{S_{xy}}{S_x \cdot S_y} = \frac{\sum_{i=1}^{n}\left(x_i - \overline{X}\right)\cdot\left(y_i - \overline{Y}\right)}{\sqrt{\left(\sum_{i=1}^{n}\left(x_i - \overline{X}\right)^2\right)\cdot\left(\sum_{i=1}^{n}\left(y_i - \overline{Y}\right)^2\right)}} = 0.9992 \tag{6}$$

where $S_x = \sqrt{\frac{1}{n-1}\sum_{i=1}^{n}\left(x_i - \overline{X}\right)^2} = 31.898$ and $S_y = \sqrt{\frac{1}{n-1}\sum_{i=1}^{n}\left(y_i - \overline{Y}\right)^2} = 3.78 \cdot 10^3$ represent the standard deviations of X and Y vectors values, respectively, which return the square root of the sample variance of X and Y elements. Therefore, the variance of X and Y values, defined as the square of the standard deviations, is calculated to determine the sample variances:

$$S_x^2 = \frac{1}{n-1}\sum\left(x_i - \overline{X}\right)^2 = 1.017 \cdot 10^3 \tag{7}$$

$$S_y^2 = \frac{1}{n-1}\sum_{i=1}^{n}\left(y_i - \overline{Y}\right)^2 = 1.428 \cdot 10^7 \tag{8}$$

Also, an important factor in statistics is the coefficient of determination, denoted by R^2, which quantifies the variation proportion in the dependent variable (determined on the basis of the independent variable). This coefficient provides a measure of how adequate the observed results are replicated by the model, based on the proportion of the total variation in the results explained by the model (Draper & Smith, 1998; Glantz, Slinker & Neilands, 2001).

For the linear model treated in this statistic, where only one intercept is included, R^2 is the square of the correlation coefficient (R) between the observed outcomes and the observed values of the predictors (Devore, 2015). This coefficient of determination ranges from 0 to 1, and in the case of measured data is:

$$R^2 = \left(0.9992\right)^2 \approx 0.998 \tag{9}$$

Figure 2 shows the engine performance curve without a mounted propeller resulting from the tachometer measurements, and Figure 3 shows a linear regression of the revolutions in comparison with the engine throttle without a mounted propeller by employing the least squares method, using the data registered.

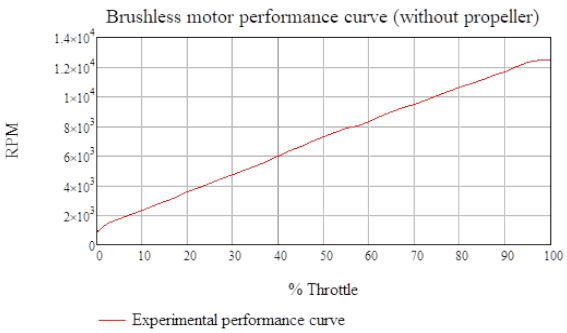

Figure 2. Engine performance curve without mounted propeller resulting from measurements

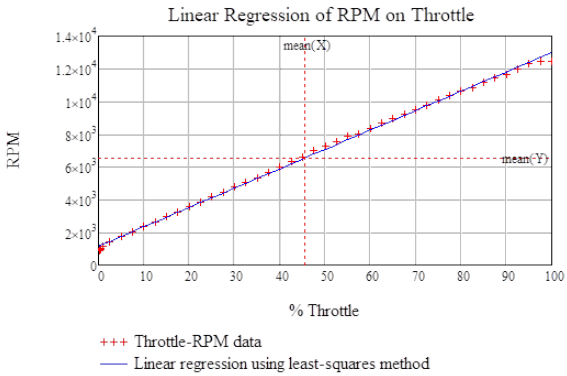

Figure 3. Linear regression using least squares method of engine speed vs. throttle gear

The correlation coefficient must be interpreted after examining the scatterplot to eliminate situations where systematic distributions appear, which would imply the existence of a non-linear relationship between X and Y. Thus, Figure 4 shows the diagram of the residuals resulting from analysing the least squares linear regression curves in Figure 3.

The correlation coefficient R always checks:

$$-1 \le r \le 1 \qquad (10)$$

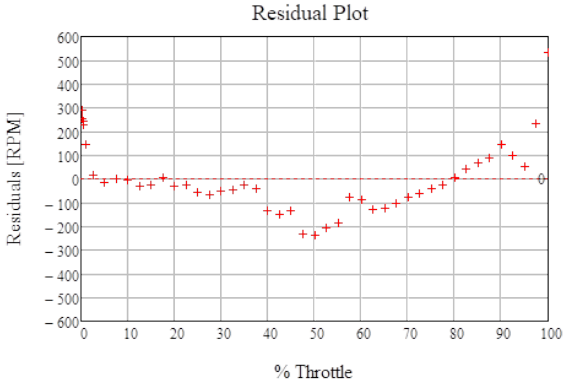

Figure 4. Residual diagram

This coefficient is R=1 or R=-1 only when the points $(x_1,y_1),...,(x_n,y_n)$ lie on a straight line. If it is 1, then the scatter diagram points lie on a straight line of increasing slope, and if it is -1, then the points of the scatterplot are located on a line of decreasing slope. When the correlation coefficient R has a value close to 1 or -1, it means that there is a (linear) dependence between the values $x_1,..., x_n$ and $y_1,..., y_n$. It can be shown that if R has a value close to 0, then there is no such relationship between those values.

Obtaining a correlation coefficient, in the performed calculations, it can be observed that, in absolute value, it tends to 1, which means that the intensity of the linear relationship between the two variables X and Y is high (the dispersion of the points is relatively small). Also, with a value > 0 (which belongs to the range (0,1)), in the relationship between X and Y, for an increase in X, an increase in Y was also determined, achieving a positive relationship (the point cloud could be adjusted to a line with an increasing – positive slope). After obtaining the residual values shown in the residual diagram, a residual histogram was created (Figure 5). For its representation, Mathcad software was used again, from which the number of points corresponding to the 10 intervals of RPM values of the residuals (shown in Table 1, with each interval accumulating 77.1729 RPMs) were obtained.

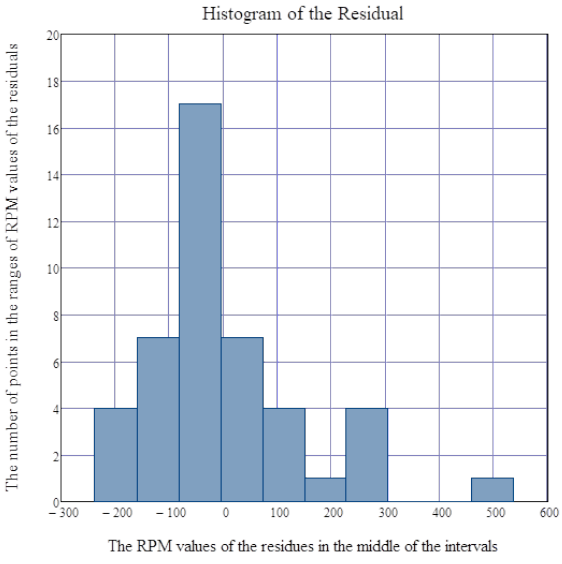

Figure 5. Residual histogram

Table 1. The number of points corresponding to the 10 intervals of RPM values of the residuals

Intervalnumber	The intervals of RPM values of the residuals reported on the regression line	The average speed [RPM] value of the interval	The number of points contained in the RPM values intervals of the residuals
1	(-236.516) – (-159.343)	-197.930	4
2	(-159.343) – (-82.170)	-120.757	7
3	(-82.170) – (-4.997)	-43.584	17
4	(-4.997) – (72.176)	33.589	7
5	(72.176) – (149.349)	110.762	4
6	(149.349) – (226.522)	187.935	1
7	(226.522) – (303.695)	265.108	4
8	(303.695) – (380.868)	342.281	0
9	(380.868) – (458.041)	419.454	0
10	(458.041) – (535.213)	496.627	1

3.2 Engine Speed with Mounted Propeller

Forwards are presented the performance curves of the electric motor with mounted propeller, registered from the tachometer measurements.

Several types of regressions were made on the recorded data for the engine with the mounted propeller, namely a linear regression and six types of univariate polynomial regressions using the least squares method, thus obtaining a regression line and several polynomial regression curves and the residuals graphs (errors).

Figure 6 shows the motor performance curve with the mounted propeller resulting from the tachometer measurements, using the recorded data.

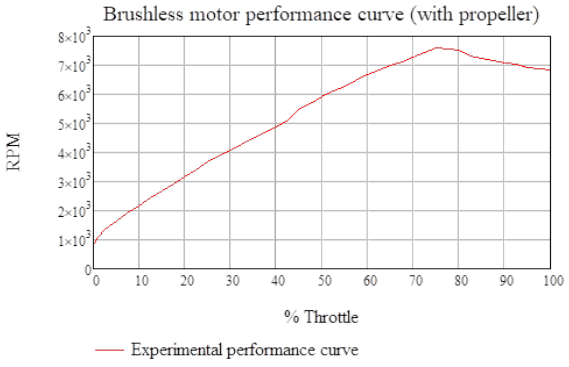

Figure 6. Performance curve of engine with mounted propeller resulting from measurements

It can be seen that for the RPM values recorded by the tachometer on the engine with the mounted propeller, a linear regression does not give the best results because the residuals show large deviations from the regression line, therefore a polynomial regression was recommended to determine a curve of regression to fit the recorded data as well as possible.

The linear regression function will provide an equation also of the form Equation (1).

For the linear regression performed on the data recorded with the tachometer on the engine with the mounted propeller, the following values were calculated:

$$b_0 = \bar{Y} - b_1 \cdot \bar{X} = 1.766 \cdot 10^3 \quad (11)$$

$$b_1 = \frac{\sum\left(x_i - \bar{X}\right)\left(y_i - \bar{Y}\right)}{\left(x_i - \bar{X}\right)^2} = 68.427 \quad (12)$$

Standard error of estimate:

$$s = \sqrt{\frac{1}{n-2}\sum\left[y_i - (b_0 + b_1 \cdot x_i)\right]^2} = 717.542 \quad (13)$$

Covariance:

$$S_{xy} = \frac{1}{n-1}\sum_{i=1}^{n}\left(x_i - \bar{X}\right)\cdot\left(y_i - \bar{Y}\right) = 6.634 \cdot 10^4 \quad (14)$$

Correlation coefficient:

$$R = \frac{S_{xy}}{S_x \cdot S_y} = \frac{\sum_{i=1}^{n}\left(x_i - \bar{X}\right)\cdot\left(y_i - \bar{Y}\right)}{\sqrt{\left(\sum_{i=1}^{n}\left(x_i - \bar{X}\right)^2\right)\cdot\left(\sum_{i=1}^{n}\left(y_i - \bar{Y}\right)^2\right)}} = 0.9499 \quad (15)$$

Standard deviations:

$$S_x = \sqrt{\frac{1}{n-1}\sum_{i=1}^{n}\left(x_i - \bar{X}\right)^2} = 31.498 \quad (16)$$

and

$$S_y = \sqrt{\frac{1}{n-1}\sum_{i=1}^{n}\left(y_i - \bar{Y}\right)^2} = 2.269 \cdot 10^3 \quad (17)$$

Variants:

$$S_x^{\,2} = \frac{1}{n-1}\sum_{i=1}^{n}\left(x_i - \bar{X}\right)^2 = 992.094 \quad (18)$$

and

$$S_y^{\,2} = \frac{1}{n-1}\sum_{i=1}^{n}\left(y_i - \bar{Y}\right)^2 = 5.148 \cdot 10^6 \quad (19)$$

Coefficient of determination:

$$R^2 = \left(0.9499\right)^2 \approx 0.902 \quad (20)$$

Figure 7 shows a linear regression of the revolutions as a function of the engine throttle using the least squares method, and Figure 8 shows the diagram of the residuals resulting from the analysis of the linear regression curve by employing the least squares method from Figure 7.

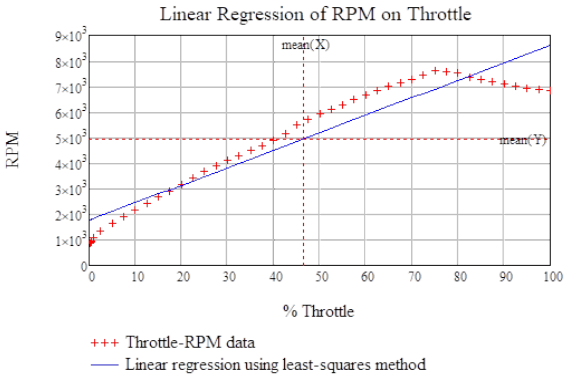

Figure 7. Linear regression using least squares method of engine speed vs. throttle gear

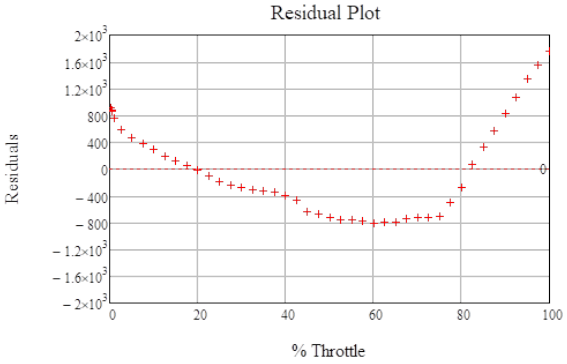

Figure 8. Residuals diagram

For the residual histogram (Figure 9), the number of points corresponding to the 10 intervals of RPM values of the residuals (shown in Table 2, with each interval accumulating 255.9085 RPMs) were obtained.

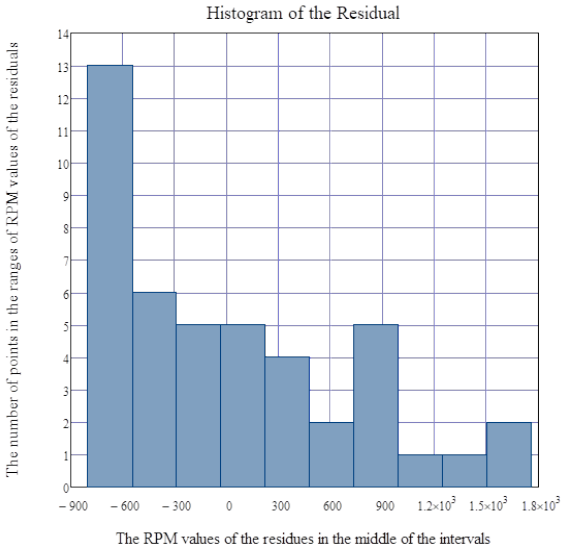

Figure 9. Residual histogram

Polynomial regression is a form of regression analysis in which the relationship between the

Table 2. The number of points corresponding to the 10 intervals of RPM values of the residuals for regression using 1st order polynomial function

Interval number	The intervals of RPM values of the residuals reported on the regression line	The average speed [RPM] value of the interval	The number of points contained in the RPM values intervals of the residuals
1	(-803.999) – (-548.091)	-676.045	13
2	(-548.091) – (-292.182)	-420.136	6
3	(-292.182) – (-36.274)	-164.228	5
4	(-36.274) – (219.635)	91.681	5
5	(219.635) – (475.544)	347.589	4
6	(475.544) – (731.452)	603.498	2
7	(731.452) – (987.361)	859.406	5
8	(987.361) – (1243.269)	1,115.315	1
9	(1243.269) – (1499.178)	1,371.223	1
10	(1499.178) – (1755.086)	1,627.132	2

independent variables X and the dependent variables Y is modelled in the polynomial of degree n ($n = 2, 3, 4, 5$ in the present case) in X.

Although polynomial regression fits a nonlinear model of the data, a statistical estimation problem is linear, in the sense that the regression function is linear in the unknown parameters that are estimated from the data. For this reason, polynomial regression is considered to be a special case of multiple linear regression, and, as with linear regression models, polynomial regression models are also often fitted by the least squares method (the least squares method minimizing the variance of the coefficients, according to the Gauss-Markov theorem). Thus, through this type of regression, an adjustment of the polynomial equation is performed on the measured data, maintaining a curvilinear relationship between the dependent and independent variables.

The polynomial regression function will provide an equation of the form:

$$Y = r(X) = a_0 + a_1 \cdot X + a_2 \cdot X^2 + ... + a_n \cdot X^n \quad (21)$$

where:

X = column vector of throttle percentage values (predictor variables), Y = column vector of RPM values (predicted, estimated variables), a_0 = the free term of the regression curve (the value for $X=0$), and $a_1,...,a_n$ = regression coefficients (amount by which Y changes when X changes by one unit).

In matrix form, the model becomes:

$$\begin{bmatrix} y_1 \\ y_2 \\ y_3 \\ \vdots \\ y_n \end{bmatrix} = \begin{bmatrix} 1 & x_1 & x_1^2 & \dots & x_1^m \\ 1 & x_2 & x_2^2 & \dots & x_2^m \\ 1 & x_3 & x_3^2 & \dots & x_3^m \\ \vdots & \vdots & \vdots & \ddots & \vdots \\ 1 & x_n & x_n^2 & \cdots & x_n^m \end{bmatrix} \cdot \begin{bmatrix} a_1 \\ a_2 \\ a_3 \\ \vdots \\ a_n \end{bmatrix} \quad (22)$$

In the present case, it is noted that there is only one independent variable, X, and the shape of the relationship between Y and X is curvilinear, as suggested by the scatterplot.

The first approach to the polynomial regression curve is quadratic, thus a loess function was performed in Mathcad software. This function was selected to fit a series of quadratic functions to the measured data using local regression. The loess function tries to fit different quadratic polynomials depending on the point situated on the curve. It does this by examining data from a small vicinity of the point of interest. The span argument controls the size of this vicinity. As the interval gets larger, loess becomes equivalent to the regress function with $n = 2$. This loess function returns a vector that the interp function uses to find a set of second-order polynomials that best fit in the vicinity of the x and y data values of X and Y by employing the least squares method.

Being controlled by the span, the size of the vicinities determined its choice of 0.4 to obtain a curve shape as close as possible to the desired shape.

The downside of choosing a larger span value is that the vicinity of the fits made by the loess function becomes smoother, as fewer points will be connected in the adjustment made, thus the fit fails to follow the features of the data properly. Also, as the interval becomes smaller, it is observed that the loess function does not converge.

The interp function returns the interpolated y value corresponding to x using the output vector from the loess function (Figure 10).

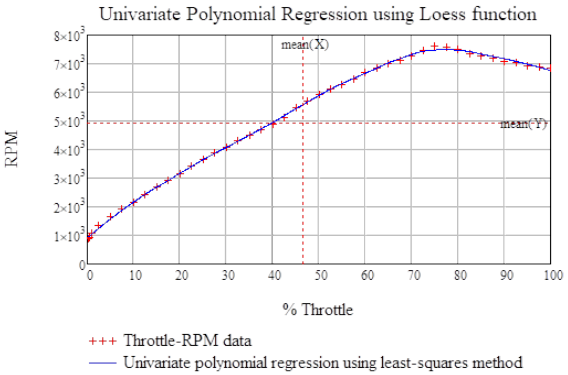

Figure 10. Polynomial regression using Loess function of engine speed vs. throttle gear

The regress function in Mathcad returns a vector that the interp function uses to find the n-order polynomial that best fits the x and y data values in X and Y in a least-squares sense. The output of the function is a vector containing the identifiers of the variables as well as the polynomial coefficients. Given that the loess function is used to perform a localized regression, regress matches better on the measured data because it fits all points in the recorded data using a single polynomial. Therefore, Figure 11 shows the regression curves with polynomial functions of 2nd, 3rd, 4th and 5th degree.

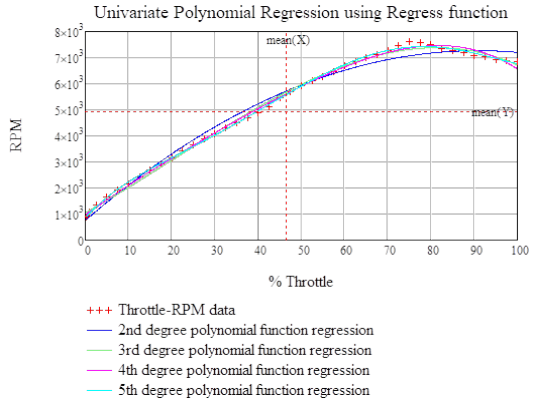

Figure 11. Polynomial regression using *Regress* function of engine speed vs. throttle gear

To extract the specific coefficients associated with the individual monomial terms in the model function (instead of letting interp create the function internally), two programs made in Mathcad were used. Thus, the obtained polynomial functions are the following:

2nd degree polynomial function:

$$Y = r(X) = 752.501 + 143.347 \cdot X - \\ -0.789 \cdot X^2 \quad (23)$$

3rd degree polynomial function:

$$Y = r(X) = 1.045 \cdot 10^3 + 92.775 \cdot X + \\ +0.591 \cdot X^2 - 9.512 \cdot 10^{-3} \cdot X^3 \quad (24)$$

4th degree polynomial function:

$$Y = r(X) = 962.761 + 120.026 \cdot X - \\ -0.783 \cdot X^2 + 0.013 \cdot X^3 - 1.141 \cdot 10^{-4} \cdot X^4 \quad (25)$$

5th degree polynomial function:

$$Y = r(X) = 853.535 + 180.671 \cdot X - 5.618 \cdot X^2 + \\ +0.149 \cdot X^3 - 1.68 \cdot 10^{-3} \cdot X^4 + 6.336 \cdot 10^{-6} \cdot X^5 \quad (26)$$

After obtaining the values of the residuals shown in Figure 12, Figure 14, Figure 16 and Figure 18, the histograms of the residuals were created (Figure 13, Figure 15, Figure 17 and Figure 19).

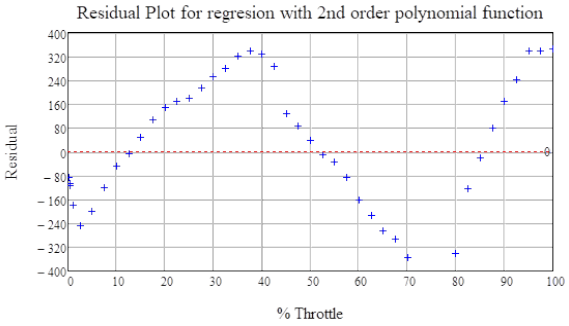

Figure 12. Residual diagram for regression using 2nd order polynomial function

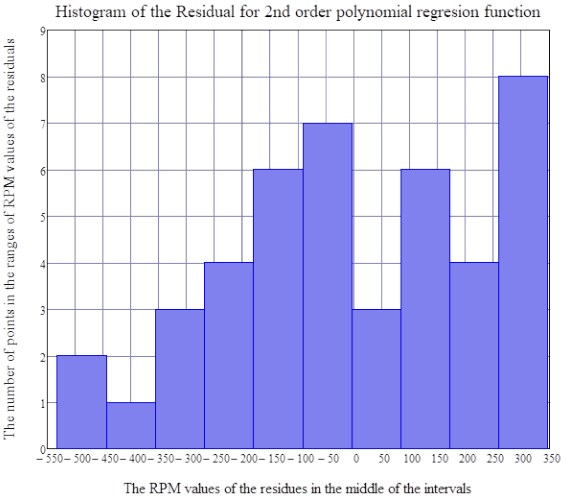

Figure 13. Residual histogram for regression using 2nd order polynomial function

Table 3. The number of points corresponding to the 10 intervals of RPM values of the residuals for regression

Interval number	The intervals of RPM values of the residuals reported on the regression line	The average speed [RPM] value of the interval	The number of points contained in the RPM values intervals of the residuals
1	(-532.019) – (-444.216)	-488.117	2
2	(-444.216) – (-356.414)	-400.315	1
3	(-356.414) – (-268.611)	-312.512	3
4	(-268.611) – (-180.808)	-224.709	4
5	(-180.808) – (-93.005)	-136.907	6
6	(-93.005) – (-5.203)	-49.104	7
7	(-5.203) – (82.600)	38.699	3
8	(82.600) – (170.403)	126.501	6
9	(170.403) – (258.205)	214.304	4
10	(258.205) – (346.008)	302.106	8

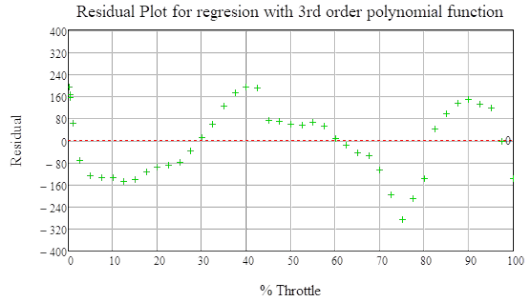

Figure 14. Residual diagram for regression using 3rd order polynomial function

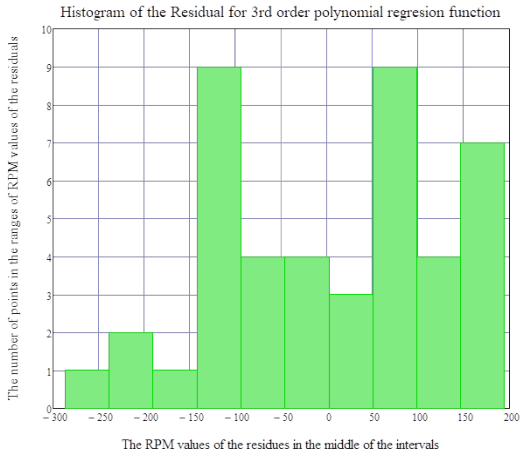

Figure 15. Residual histogram for regression using 3rd order polynomial function

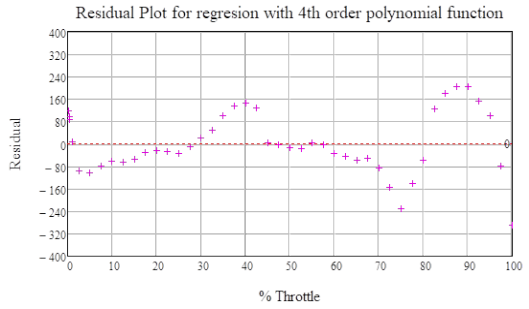

Figure 16. Residual diagram for regression using 4th order polynomial function

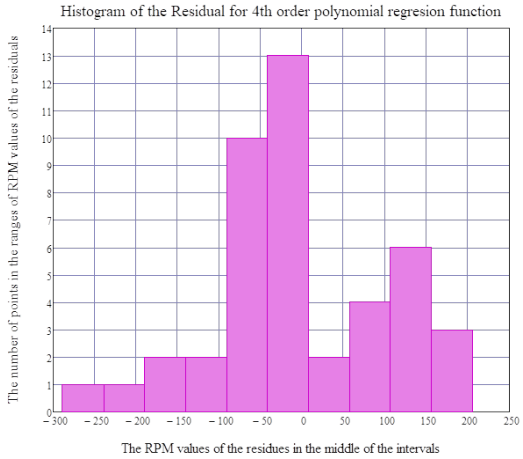

Figure 17. Residual histogram for regression using 4th order polynomial function

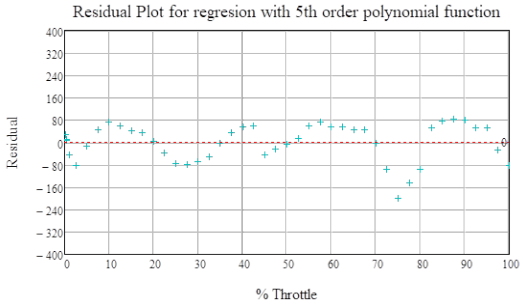

Figure 18. Residual diagram for regression using 5th order polynomial function

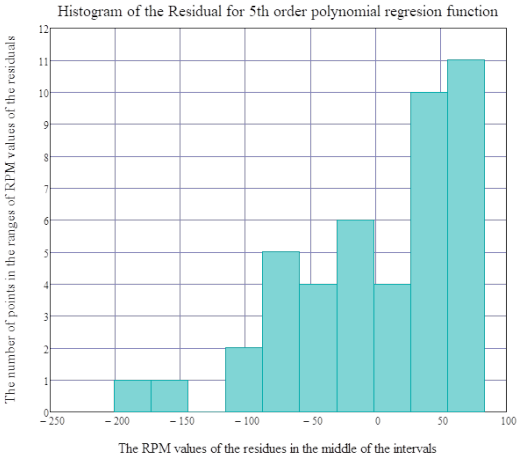

Figure 19. Residual histogram for regression using 5th order polynomial function

For the representations of these histograms, Mathcad software was again used, from which the number of points corresponding to the 10 intervals of RPM values of the residuals (presented in Table 3, with each interval accumulating 87.8027 RPMs, in Table 4, with each interval accumulating 48.1712 RPM, in Table 5, with each interval accumulating 49.3121 RPM, and in Table 6, with each interval accumulating 28.4806 RPM, respectively) were obtained.

It can be seen that the regression with a 5th order polynomial function passes through several points of the Throttle-RPM data, and the errors (residuals) are found at relatively small distances in comparison with the regression curve.

For regressions with polynomial functions of lower degree, it can be observed that the residuals show larger distances compared to the regression curves.

For regressions with polynomial functions of higher degree the model captures noise in the generated data, thus creating an over-fitting.

Table 4. The number of points corresponding to the 10 intervals of RPM values of the residuals for regression using 3rd order polynomial function

Interval number	The intervals of RPM values of the residuals reported on the regression line	The average speed [RPM] value of the interval	The number of points contained in the RPM values intervals of the residuals
1	(-286.916) – (-238.745)	-262.831	1
2	(-238.745) – (-190.574)	-214.659	2
3	(-190.574) – (-142.402)	-166.488	1
4	(-142.402) – (-94.231)	-118.317	9
5	(-94.231) – (-46.060)	-70.146	4
6	(-46.060) – (2.111)	-21.975	4
7	(2.111) – (50.282)	26.197	3
8	(50.282) – (98.454)	74.368	9
9	(98.454) – (146.625)	122.539	4
10	(146.625) – (194.796)	170.71	7

Table 5. The number of points corresponding to the 10 intervals of RPM values of the residuals for regression using 4rd order polynomial function

Interval number	The intervals of RPM values of the residuals reported on the regression line	The average speed [RPM] value of the interval	The number of points contained in the RPM values intervals of the residuals
1	(-288.453) – (-239.141)	-263.797	1
2	(-239.141) – (-189.829)	-214.485	1
3	(-189.829) – (-140.517)	-165.173	2
4	(-140.517) – (-91.205)	-115.861	2
5	(-91.205) – (-41.893)	-66.549	10
6	(-41.893) – (7.420)	-17.236	13
7	(7.420) – (56.732)	32.076	2
8	(56.732) – (106.044)	81.388	4
9	(106.044) – (155.356)	130.7	6
10	(155.356) – (204.668)	180.012	3

Table 6. The number of points corresponding to the 10 intervals of RPM values of the residuals for regression using 5rd order polynomial function

Interval number	The intervals of RPM values of the residuals reported on the regression line	The average speed [RPM] value of the interval	The number of points contained in the RPM values intervals of the residuals
1	(-201.210) – (-172.729)	-186.969	1
2	(-172.729) – (-144.249)	-158.489	1
3	(-144.249) – (-115.768)	-130.008	0
4	(-115.768) – (-87.288)	-101.528	2
5	(-87.288) – (-58.807)	-73.047	5
6	(-58.807) – (-30.326)	-44.567	4
7	(-30.326) – (-1.846)	-16.086	6
8	(-1.846) – (26.635)	12.394	4
9	(26.635) – (55.115)	40.875	10
10	(55.115) – (83.596)	69.356	11

4. Determination of the Thrust Force Developed by the Motor-Propeller Assembly in the Brushless Motor Operating Regimes

In order to determine the thrust force that the motor-propeller assembly develops in the operating modes of the brushless electric motor, a series of tests were carried out in which two strain gauges were used to make a Wheatstone half-bridge (Patel & Srinivas, 2012). For this configuration, a strain gauge was mounted on the upper part of the beam, and the second one on the lower part (Ajovalasit, 2010). The connection of the half-bridge through the strain gauges to the MX1615B module from HBM, for recording the relative elongation parameters (micro-epsilon = ε_μ), was realized through a half-bridge circuit with 5 wires connected according to the model in Figure 20 (HBM, n.d.). A schematic of the experimental stand is presented in Figure 21.

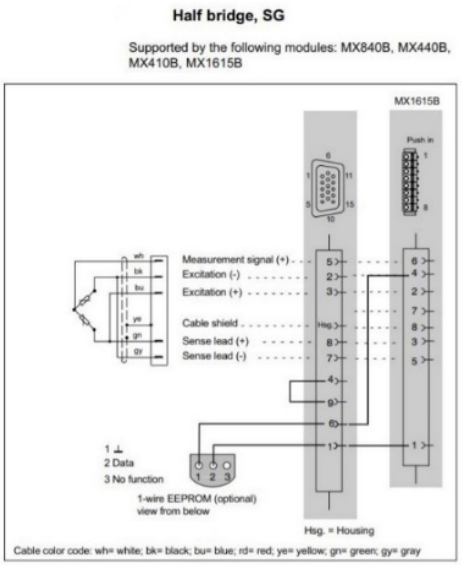

Figure 20. Connecting the Wheatstone half bridge to HBM's MX1615B module (HBM, n.d.)

In the schematization presented in Figure 21, the geometric characteristics have the following numerical values:

- $L_{strain\_gauge\_position}$=0.24m;
- L_{arm}=0.275m;
- R=0.008m;
- r=0.007m;
- E =3.897·10[10]Pa = the carbon tube modulus of elasticity;
- $I = \frac{\pi\left(R^4 - r^4\right)}{4} = 1.331 \cdot 10^{-9}\, m^4$ = moment of inertia;
- $F_{analitical} = \frac{2E \cdot I}{L_{arm} \cdot R} \cdot \varepsilon = 4.716 \cdot 10^4\, N \cdot \varepsilon =$ thrust force developed by the engine.

The strain gauge data record is the one of the relative micro-elongation ε_μ whose measurement unit is $[\mu m/m]$, which means that $\varepsilon=\varepsilon_\mu \cdot 106$, and

$$F_{analitical} = \frac{2E \cdot I}{L_{arm} \cdot R} \cdot 10^{-6} \cdot \varepsilon = 0.04716 \cdot \varepsilon_\mu .$$

Following the acquisition system calibration, the ratio $\frac{2E \cdot I}{L_{arm} \cdot R} = 0.05274194$, therefore a comparison of the thrust force results was performed.

With the values obtained from the measurements made with the Wheatstone half-bridge, the following graphs were drawn: the analytical and real performance curves of the motor-propeller assembly shown in Figure 22 and the analytical and real thrust developed by the motor-propeller assembly as a function of speed shown in Figure 23.

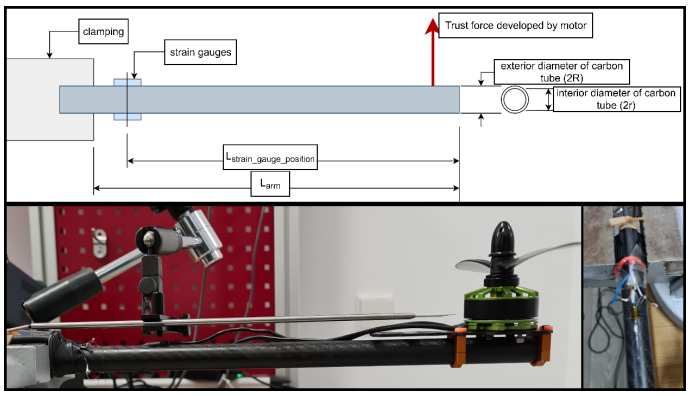

Figure 21. Schematic of the quadcopter arm regarding the location of the strain gauges and the physical realization of the assembly

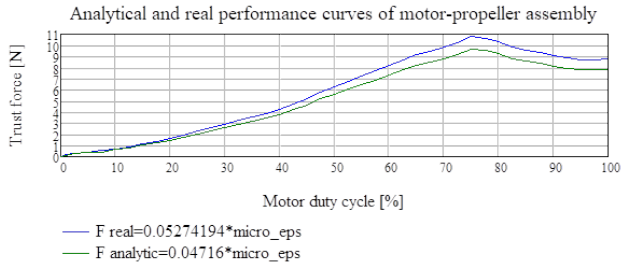

Figure 22. Analytical and real performance curves of the motor-propeller assembly

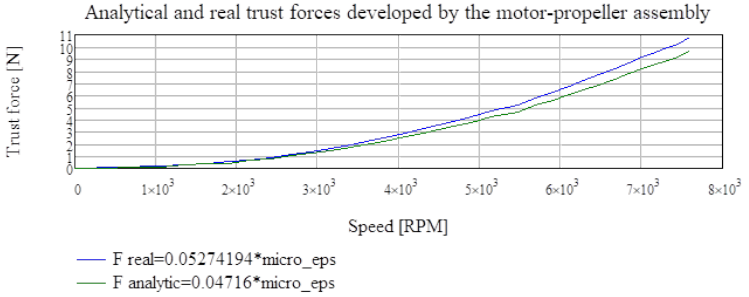

Figure 23. Analytical and real thrust forces developed by the motor-propeller assembly as a function of speed

5. Conclusion

Regression analysis is a statistical tool for investigating relationships between variables, multiple regression analysis being a very good method for generating mathematical models in which several variables are considered. The polynomial regression model consists of successive power terms, each model including the highest-order term plus all lower-order terms. Polynomial regression can be seen as a particular case of multiple linear regression, thus polynomial models are considered efficient curve fitting techniques.

The most used regression analysis method is the least squares analysis, which is also used in this paper. This method works by creating a line of „best fit" through all available data points, and the parameter estimates are chosen to minimize sum-of-squares errors.

The determination of the brushless motor performance curves for the rotary-wing drones was carried out with the aim of correlating the data on the motor operating regime with the response of the structure to the traction force developed by the motor-propeller assembly. The mathematical analysis of data correlation on duty cycles with rotor rotation speed was carried out using curves fitting and smoothing functions, and the determination of the traction force developed by the engine-propeller assembly was carried out using a Wheatstone half-bridge with strain gauges.

Acknowledgements

This work has been funded by the European Social Fund from the Sectoral Operational Programme Human Capital 2014-2020, through the Financial Agreement entitled "Training of PhD students and postdoctoral researchers in order to acquire applied research skills – SMART", Contract no. 13530/16.06.2022 – SMIS code: 153734.

REFERENCES

Ajovalasit, A. (2010) Advances in Strain Gauge Measurement on Composite Materials. *Strain*. 47(4), 313–325. doi: 10.1111/j.1475-1305.2009.00691.x.

Austin, R. (2010) *Unmanned Aircraft Systems: UAVS Design, Development and Deployment. Hoboken*, NJ, USA, John Wiley & Sons, Inc.

Ayamga, M., Akaba, S. & Apotele Nyaaba, A. (2021) Multifaceted applicability of UAVs: A review. *Technological Forecasting and Social Change*. 167, 120677. doi: 10.1016/j.techfore.2021.120677.

Balestrieri, E., Daponte, P., De Vito, L. & Lamonaca, F. (2021) Sensors and Measurements for Unmanned Systems: An Overview. *Sensors*. 21, 1518. doi: 10.3390/s21041518.

Daponte, P., De Vito, L., Mazzilli, G., Picariello, F. & Rapuano, S. (2017) A height measurement uncertainty model for archaeological surveys by aerial photogrammetry. *Measurement*. 98, 192–198.

Devore, J. L. (2015) *Probability and Statistics for Engineering and the Sciences*. 8th ed. Boston, USA, Cengage Learning - Brooks/Cole Publishing Company.

Draper, N. R. & Smith, H. (1998) *Applied Regression Analysis*. 3rd ed. Hoboken, NJ, USA, John Wiley & Sons, Inc.

Dwivedi, D., Singh, S. & Kalaiselvi, J. (2022) Impact of PWM and Duty Ratio Control on Voltage for Sic Fed Three Phase BLDC Motor Drive. In: *2022 IEEE International Conference on Power Electronics, Smart Grid, and Renewable Energy* (*PESGRE*), *02-05 January 2022*, *Trivandrum*, *India*. pp. 1-5. doi: 10.1109/PESGRE52268.2022.9715861.

Fox, S. J. (2020) The 'risk' of disruptive technology today (A case study of aviation - Enter the UAV). *Technology in Society*. 62, 101304. doi: 10.1016/j.techsoc.2020.101304.

Fu, J., Liu, G., Fan, C., Liu, Z. & Luo, H. (2022) Design and Experimental Study on Vibration Reduction of an UAV Lidar Using Rubber Material. *Actuators*. 11, 345. doi: 10.3390/act11120345.

Glantz, S. A., Slinker, B. K. & Neilands, T. B. (eds.) (2001) *Primer of Applied Regression and Analysis of Variance*. 2nd ed. New York, USA, McGraw-Hill, Inc.

HBM. (n.d.) Strain Gauge Catalog. https://www.hbm.com/fileadmin/mediapool/hbmdoc/technical/S01265.pdf [Accessed 25th August 2022].

He, D., Liu, H., Chan, S. & Guizani, M. (2019) How to Govern the Non-Cooperative Amateur UAVs?. *IEEE Network*. 33, 184–189. doi: 10.1109/MNET.2019.1800156.

International Organization for Standardization (ISO) (n.d. a) *ISO/CD 4358 Test Methods for Civil Multi-Rotor Unmanned Aircraft System*. https://www.iso.org/standard/79891.html?browse=tc [Accessed 21st May 2023].

International Organization for Standardization (ISO) (n.d. b) *ISO/AWI 5309 Vibration Test Methods for Lightweight and Small Civil UAS*. https://www.iso.org/standard/81112.html?browse=tc [Accessed 21st May 2022].

Meyer, I. Z. & Barros, J. E. (2021) Characterization of small Brushless motors for unmanned aerial vehicles. *Brazilian Journal of Development*. 7(6), 63447-63463. doi: 10.34117/bjdv7n6-631.

Otkun, Ö., Demir, F. & Otkun, S. (2022) Scalar speed control of induction motor with curve-fitting method. *Automatika*. 63(4), 618-626. doi: 10.1080/00051144.2022.2060657.

Patel, B. D. & Srinivas, A. R. (2012). Validation of Experimental Strain Measurement Technique and Development of Force Transducer. *International Journal of Scientific & Engineering Research*. 3(10), 1–4.

Petritoli, E., Leccese, F. & Ciani, L. (2018) Reliability and Maintenance Analysis of Unmanned Aerial Vehicles. *Sensors*. 18, 3171. doi: 10.3390/s18093171.

Qu, Z. & Wu, T. (2016) *Systems and Methods for Operating Unmanned Aerial Vehicles*. US20190179344A1 (Patent). https://patents.google.com/patent/US11275389B2/en [Accessed 21st May 2022].

Tofan-Negru, A., Ștefan, A., Grigore, L. Ș. & Oncioiu, I. (2023) Experimental and Numerical Considerations for the Motor-Propeller Assembly's Air Flow Field over a Quadcopter's Arm. *Drones*. 7(3), 199. doi: 10.3390/drones7030199